NASA Contractor Report 159108

EFFECTS OF REFRACTION BY MEAN FLOW VELOCITY GRADIENTS ON THE STANDING WAVE PATTERN IN THREE-DIMENSIONAL, RECTANGULAR WAVEGUIDES

Alan S. Hersh

HERSH ACOUSTICAL ENGINEERING
Chatsworth, Ca. 91311

CONTRACT NAS1-15311
JUNE 1979

National Aeronautics and
Space Administration

Langley Research Center
Hampton, Virginia 23665
AC 804 827-3966

TABLE OF CONTENTS

DEFINITION OF SYMBOLS

Symbol	Definition
A_i, A	amplitude of incident and reflected sound pressure waves respectively
A_{oo}, A_m	sound pressure coefficients defined by Eqs. (39) and (47) respectively
$A(\xi,\eta)$	function defined by Eq. (68)
B_l	sound pressure coefficient defined by Eq. (47)
$B(\xi,\eta)$	function defined by Eq. (69)
C_{ml}	sound pressure coefficient defined by Eq. (47)
$C(\xi,\eta)$	function defined by Eq. (73a)
$D(\xi,\eta)$	function defined by Eq. (73b)
E_m	sound pressure coefficient defined by Eq. (51)
f_o, f_1, f_2	non-dimensionalized perturbed sound pressures defined by Eq. (28)
F	sound pressure defined by Eq. (20)
G_{oo}, G_m	sound pressure coefficients defined by Eqs. (41) &(42) respectively
g	transverse acoustic velocity defined by Eq. (22)
H	duct height defined in Fig. (4)
H_l	sound pressure coefficient defined by Eq. (44)
h	vertical acoustic velocity defined by Eq. (21)
I_{ml}	sound pressure coefficient defined by Eq. (46)
J_l	sound pressure coefficient defined by Eq. (45)
k	sound wave number ($=\omega/c_o$)
l,m	running integers
L^2	parameter defined by Eq. (9)
M	mean flow Mach number
M_c	mean flow centerline Mach line
M_g	sound field group Mach number defined by Eq. (65)

Symbol	Definition
N	exponent on mean flow velocity profile, defined by Eq. (31)
p	acoustic pressure
R	amplitude of upstream sound pressure, defined by Eq. (7b)
u,v,w	acoustic velocites in x,y,z directions respectively
V_o	mean flow speed
V_c	mean flow center line speed
V_p	sound phase speed
V_g	sound group speed defined by Eq. (63)
W	duct width, defined in Fig. (4)
x,y,z	duct coordinates, defined in Fig. (4)
β	duct aspect ratio ($\equiv H/W$)
ξ η	duct nondimensionalized transverse coordinates defined by Eq. (26)
λ	sound wavelength
κ	system eigenvalue defined by Eq. (20)
ρ	density
ω	sound circular frequency
ϕ	phase angle shift between incident and reflected sound waves in duct, defined by Eq. (7b)

Subscripts	
o	denotes mean quantities
c	denotes duct centerline values
max	maximum value of quantity
min	minimum value of quantity

SUMMARY

The influence of a mean vortical flow on the connection between the standing wave pattern in a rectangular three-dimensional waveguide and the corresponding duct axial impedance has been determined analytically. The solution was derived using a perturbation scheme valid for low mean flow Mach numbers and plane-wave sound frequencies. The results show that deviations of the standing wave pattern due to refraction by the mean flow gradients are small.

1. INTRODUCTION

Three different methods to measure the impedance of sound absorbing liners in the presence of grazing flow have been reported in the literature[1-8]. The three methods are (1) the two-microphone method of measurement (References 1-6), (2) the impedance tube method (Reference 7) and (3) the wave guide method (Reference 8). The two-microphone method is a particularly attractive method of measuring the impedance of cavity-backed, thin facesheet liners consisting of either porous materials or perforates. Its use however, is restricted to single cavity liners - thus its application is restricted to the measurement of the impedance of only locally reacting liners.

The impedance tube method has been used successfully to measure the normal impedance of locally reacting materials in a *nongrazing flow environment*. In an attempt to apply this method in a grazing flow environment, Feder and Dean[7] experienced considerable difficulty in properly accounting for the radiation impedance losses of the sample liners mounted in the side of the flow duct facility.

Armstrong[8] outlined a waveguide method to measure the impedance of a liner installed along one side wall of a constant area rectangular duct facility with grazing flow. By assuming that the rectangular duct consisted of a source at one end and a non-reflective termination at the other, Armstrong was able to model the duct mathematically as semi-infinite with one side wall lined, the others acoustically rigid. With this assumption, he proceeded to solve for the sound field within the duct assuming a uniform mean duct flow. In this way, Armstrong was able to show a connection between the liner impedance and the sound field attenuation and phase change per unit duct length (recall that one side wall of an *entire* infinite duct was lined - thus the sound pressure decayed continuously). Straight forward measurement of the sound field attenuation and phase change per unit length with an axially mounted microphone yielded, after relatively

minor computations, prediction of the liner impedance. Although this approach appears to be straight forward, difficulties associated with flow noise in the downstream diffuser (the flow appeared to separate in the diffuser) prevented Armstrong from assessing the accuracy of the waveguide approach.

Despite the difficulties experienced by Armstrong, the wave guide approach is attractive because it will permit, at least conceptually, the measurement of the effects of flow on the impedance of *extended* liners. As noted above, the other two methods described above are restricted to locally reacting liners (by "locally reacting" from a practical viewpoint, it is meant that the size of the liner is very small compared to the wavelength). A critical aspect in the development of a waveguide method of measuring impedance in a flow duct environment is the connection between the standing wave pattern along the wave guide and the corresponding duct axial impedance. Of special interest here is the details of this connection when the mean flow is vortical. An analytical solution has been derived by restricting the Mach number of the mean flow to be small and the sound frequencies of interest to be below the first rigid-wall, zero Mach number cut-on mode - the plane wave mode. Under these restrictions, deviations of the standing wave pattern from its nongrazing flow plane wave distribution will not be large. This permits an analytic representation of the flow related standing wave pattern in terms of regular perturbations from its zero grazing flow distribution.

The use of the perturbation theory has been successfully used by Hersh and Catton[9] to study the effects of mean flow velocity gradients on the refraction of sound in infinite two-dimensional rigid-walled ducts. Their results showed good agreement with exact numerical solutions.

Within the past decade, there has been an enormous interest in understanding the manner in which sound attenuation in lined ducts is affected by flow. A rather extensive review of this subject was recently presented by Nayfey, Kaiser and Telionus[10].

Briefly, previous studies in this field can be divided into two parts, one describing the effects of flow on the propagation of sound in rigid-walled flow ducts and the other to the propagation (and attenuation) of sound in acoustically lined flow ducts.

Pridmore-Brown[11] was one of the first to study the effects of vortical flow on the propagation of sound in two-dimensional ducts. Since the publication of Pridmore-Brown's work, there has been considerable interest in the manner in which sound propagates in a vortical flow. Recent publications of interest include the work of Mungur and Gladwell[12], Mechel, Mertens and Schilz[13], Tack and Lambert[14] and Mungur and Plumblee[15]. These studies which are primarily limited to the case of downstream propagation, have results consistent with those of Pridmore-Brown.

It is intuitively clear that if the effect of mean flow shear is to refract thereby amplify the sound pressure near the duct wall for downstream sound propagation and into the duct center for upstream sound propagation, then the standing wave pattern and the corresponding duct axial impedance must take this into account.

The report is organized as follows. The solution of the standing wave pattern for the case of uniform mean flow is presented in Section 2. The basic equations governing the propagation of sound in a rigid-wall three dimensional rectangular duct containing a mean vortical flow are derived in Section 3. The analytical solution is based on application of the perturbation method described in Section 4. A detailed solution is derived in Section 5 corresponding to the special case of plane wave propagation in a square duct containing a fully-developed mean flow. The velocity profile of the mean flow was assumed to be linear. This permitted an analytic solution to be derived. The main findings of the study are summarized in Section 6.

2. UNIFORM FLOW SOLUTION

The connection between the standing wave pattern in a waveguide and the corresponding duct axial impedance is derived below for the special case of uniform duct flow. This case is important because it provides a check case for the more complicated vortical flow solution described in Section 4 and serves as an excellent introduction to the complexities associated with a vortical mean flow. The solution is presented in two parts, one in which the basic equations and the other the duct axial impedance are derived.

2.1 Basic Equations

Assume that the duct shown in Fig. 1 contains a uniform mean flow. Assume further that sound, introduced into the duct at, say, $x=-L$, generates a standing wave pattern between $x=-L$ and $x=0$. The strength of the reflected wave is a function of the duct effective axial impedance Z. The objective of the analysis is to derive a relationship between the standing wave pattern and the duct axial impedance Z with the duct mean flow speed, V_o, a parameter.

For uniform flow in a rectangular duct, the linearized continuity and momentum equations are

$$\frac{\partial \rho}{\partial t} + V_o \frac{\partial \rho}{\partial x} + \rho_o \left(\frac{\partial u}{\partial x} + \frac{\partial v}{\partial y} + \frac{\partial w}{\partial z} \right) = 0 \tag{1}$$

$$\frac{\partial u}{\partial t} + V_o \frac{\partial u}{\partial x} + \frac{1}{\rho_o} \frac{\partial p}{\partial x} = 0 \tag{2a}$$

$$\frac{\partial v}{\partial t} + V_o \frac{\partial v}{\partial x} + \frac{1}{\rho_o} \frac{\partial p}{\partial y} = 0 \tag{2b}$$

$$\frac{\partial w}{\partial t} + V_o \frac{\partial w}{\partial x} + \frac{1}{\rho_o} \frac{\partial p}{\partial z} = 0 \tag{2c}$$

Here the subscript (o) denotes mean flow quantities. Thus ρ_o and V_o represent the mean density and uniform duct speed respectively. The quantities p,ρ,u,v,w represent acoustic excitations of pressure, density, axial. transverse in y direction, and transverse in z direction velocities respectively. Assuming p and ρ are adiabatically related, Eqs. (1) and (2) may be combined to form the well known convected wave equation

$$\frac{1}{c_o^2}\frac{\partial^2 p}{\partial t^2} - \left(1 - M_o^2\right)\frac{\partial^2 p}{\partial x^2} - \frac{\partial^2 p}{\partial y^2} - \frac{\partial^2 p}{\partial z^2} + \frac{2M_o}{c_o}\frac{\partial^2 p}{\partial x \partial t} = 0 \qquad (3)$$

where $M_o = V_o / c_o$.

For frequencies below the first cut-on mode, only plane wave modes are excited in a hard-walled duct. The acoustic pressure and velocity fields excited by the source are obtained by solving Eq. (3) to yield

$$p(x,t) = A_+ e^{i(\omega t - k_+ x)} + A_- e^{i(\omega t + k_- x)} \qquad (4)$$

$$u(x,t) = \frac{A_+}{\rho_o c_o} e^{i(\omega t - k_+ x)} - \frac{A_-}{\rho_o c_o} e^{i(\omega t + k_- x)} \qquad (5)$$

where A_+ and A_- represent the (complex) amplitudes of the incident and reflected waves respectively. The wave numbers

$$k_+ = \frac{K}{1+M_o} \quad ; \quad k_- = \frac{K}{1-M_o} \quad ; \quad K \equiv \frac{\omega}{c_o} \qquad (6a,b,c)$$

represent respectively the elongation and contraction of the sound wavelength $\lambda = 2\pi c_o/\omega$ due to the mean flow. Since the objective of this analysis is to derive an analytic expression connecting the impedance of a specimen located effectively at $x=0$ to the duct

mean flow speed, no loss of generality results by setting

$$A_+ \equiv 1 \quad \text{and} \quad A_- \equiv R e^{i\phi} \tag{7a,b}$$

The time-averaged pressure standing wave distribution along the duct follows immediately from Eq. (4) upon substitution of Eqs. (6) & (7),

$$\overline{p^2(x)} = 1 + R^2 + 2R \cos\left[\frac{2Kx}{1-M^2} + \phi\right] \tag{8}$$

Equation (8) describes the output of a microphone at location x - see Figure 2. The impedance of the specimen is assumed to be located at x=0. It contains two unknowns, R the amplitude of the reflected wave and ϕ the phase shift between the incident and reflected wave. Referring to the standing wave pattern shown in Fig. 2, L^2 is defined as

$$L^2 \equiv \left| \frac{\overline{p^2}_{max}}{\overline{p^2}_{min}} \right| \tag{9}$$

where from Eq. (8) the maximum and minimum values occur at the corresponding maximum and minimum values of $\cos\left(\frac{2Kx}{1-M_o^2} + \phi\right)$. Thus,

$$L^2 = \left| \frac{1+R}{1-R} \right|^2 \longrightarrow R = \frac{L-1}{L+1} \tag{10}$$

The phase angle ϕ follows immediately from Eq. (8) by measuring the distance d_1 between the specimen at x=0 and the <u>first pressure minimum</u> (see Fig. 2),

$$\frac{2Kd_1}{1-M_o^2} + \phi = \pi \longrightarrow \phi = \pi - \frac{2Kd_1}{1-M_o^2} \tag{11}$$

2.2 Impedance

In the absence of a reflected wave (see Fig. 1), the effective impedance of a specimen located at x=0 is defined as the ratio of the acoustic pressure to axial acoustic velocity. Using this definition and substituting Eqs. (4)-(7) yields

$$\mathcal{Z} \equiv \frac{p(o,t)}{u(o,t)} = \rho_o c_o \left[\frac{1 + Re^{i\phi}}{1 - Re^{i\phi}}\right] \tag{12}$$

Separating Z into its real and imaginary parts,

$$\frac{\mathcal{Z}}{\rho_o c_o} = \underbrace{\left[\frac{1-R^2}{1+R^2-2R\cos\phi}\right]}_{\text{resistance}} + i \underbrace{\left[\frac{2R\sin\phi}{1+R^2-2R\cos\phi}\right]}_{\text{reactance}} \tag{13}$$

To verify the validity of Eq. (13), three different check cases will be applied. They are (1) rigid wall impedance, $R=1, \phi=0$, (2) pressure release surface, $R=1, \phi=\pi$ and (3) no reflected wave case (i.e., $\rho_o c_o$ effective impedance), $R=\phi=0$.

$$\text{Case (1):} \quad \mathcal{Z}(R=1, \phi=0) = \frac{1-R^2}{(1-R)^2} = \frac{1+R}{1-R} \longrightarrow \infty \tag{14a}$$

$$\text{Case (2)} \quad \mathcal{Z}(R=1, \phi=\pi) = \frac{1-R^2}{(1+R)^2} = \frac{1-R}{1+R} = 0 \tag{14b}$$

$$\text{Case (3):} \quad \mathcal{Z}(R=0, \phi=0) = 1 \tag{14c}$$

It is clear from the above that Eq. (13) appears reasonable.

Solving for the resistance and reactance in terms of the parameters L^2 and d_1 results in

$$\frac{R}{\rho_o c_o} = \frac{2L}{L^2\left[1+\cos\left(\frac{Kd_1}{1-M^2}\right)\right]+\left[1-\cos\left(\frac{Kd_1}{1-M^2}\right)\right]} \tag{15}$$

$$\frac{X}{\rho_o c_o} = \frac{\left(L^2-1\right)\sin\left(\frac{Kd_1}{1-M^2}\right)}{L^2\left[1+\cos\left(\frac{Kd_1}{1-M^2}\right)\right]+\left[1-\cos\left(\frac{Kd_1}{1-M^2}\right)\right]} \tag{16}$$

Equations (15) and (16) show that the mean flow reduces the effective wavelength of the incident sound via the $\cos\left(\frac{Kd_1}{1-M^2}\right)$ term. This can be seen by replacing $K = \frac{\omega}{c_o} = \frac{2\pi}{\lambda}$, thus

$$\cos\left(\frac{Kd_1}{1-M^2}\right) = \cos\left[\frac{2\pi d_1}{\lambda\left(1-M^2\right)}\right] = \cos\left(\frac{2\pi d_1}{\lambda_{eff}}\right) \tag{17}$$

where $\lambda_{eff} = \lambda\left(1-M^2\right)$

3. VORTICAL MEAN FLOW CASE - BASIC EQUATIONS

In a real duct flow environment the duct flow speed is not uniform but instead contains the boundary layer region wherein the velocity profile varies from zero at the duct walls to an almost maximum value at the layer outer edge. The principal effect of the boundary layer region is to refract the sound pressure into the wall for sound propagating in the same direction as the duct flow (the downstream case - see Fig. 3a) and into the duct center for sound propagating in the direction opposite to the duct flow (the upstream case - see Fig. 3b).

The basic equations derived in Section 2 governing the propagation of sound in rigid-walled rectangular ducts containing a mean flow are generalized below to apply to vortical mean flow. Figure 4 is a schematic of the rectangular duct geometry and coordinate system used in the derivation.

The equations governing the conservation of mass and momentum flux in the y and z directions are identical to Eqs. (1), (2b) and (2c) respectively. The x-component of the momentum flux conservation equation, however, takes on the following form

$$\frac{\partial u}{\partial t} + V_o \frac{\partial u}{\partial x} + \left(\frac{\partial V_o}{\partial y}\right) v + \left(\frac{\partial V_o}{\partial z}\right) w + \frac{1}{\rho_o} \frac{\partial p}{\partial x} = 0 \qquad (18)$$

The convected wave equation is solved in the usual way to become

$$\underbrace{\frac{1}{c_o^2} \frac{\partial^2 p}{\partial t^2} - \left(1-M_o^2\right) \frac{\partial^2 p}{\partial x^2} - \frac{\partial^2 p}{\partial y^2} - \frac{\partial^2 p}{\partial z^2} + \frac{2M_o}{c_o} \frac{\partial^2 p}{\partial x \partial t}}_{\text{uniform flow part}} - 2\rho_o c_o \underbrace{\left[\frac{\partial M_o}{\partial y} \frac{\partial v}{\partial x} + \frac{\partial M_o}{\partial z} \frac{\partial w}{\partial x}\right]}_{\text{shear flow part}} = 0 \qquad (19)$$

The following wave-like solution to Eq. (19) is proposed based on a generalization of Pridmore-Brown's approach,

$$p\left(x, y, z; t; \kappa; V_o\right) = e^{i\omega\left(t - \frac{\kappa x}{c_o}\right)} F\left(y, z; \kappa; V_o\right) \qquad (20)$$

$$v\left(x, y, z; t; \kappa; V_o\right) = e^{i\omega\left(t - \frac{\kappa x}{c_o}\right)} g\left(y, z; \kappa; V_o\right) \qquad (21)$$

$$w\left(x, y, z; t; \kappa; V_o\right) = e^{i\omega\left(t - \frac{\kappa x}{c_o}\right)} h\left(y, z; \kappa; V_o\right) \qquad (22)$$

Here κ is the system eigenvalue. It will be shown later to be related to the group velocity of the propagating sound field. Note that the acoustic pressure and transverse velocities are written to depend explicitly upon the mean flow V_o. The functions g and h can be immediately related to F by substitution into the transvers momentum equations [see Eqs. (2b)] to yield

$$g\left(y, z; \kappa; V_o\right) = \frac{-\frac{\partial F}{\partial y}\left(y, z; \kappa; V_o\right)}{i\rho_o \omega\left(1 - \kappa M_o\right)} \qquad (23)$$

$$h(y,z;\kappa;V_o) = \frac{-\frac{\partial F}{\partial z}(y,z;\kappa;V_o)}{i\rho_o\omega\,(1-\kappa M_o)} \tag{24}$$

Substitution of Eqs. (20) thru (24) into Eq. (20) results in the following form of the wave equation,

$$\frac{\partial^2 F}{\partial y^2}+\frac{\partial^2 F}{\partial z^2}+\frac{2\kappa}{(1-\kappa M_o)}\left[\frac{\partial M_o}{\partial y}\frac{\partial F}{\partial y}+\frac{\partial M_o}{\partial z}\frac{\partial F}{\partial z}\right]+\left(\frac{\omega}{c_o}\right)^2\left[(1-\kappa M_o)^2-\kappa^2\right]F=0 \tag{25}$$

It is convenient to non-dimensionalize Eq. (25) by letting

$$F(y,z;\kappa;V_o)=P_{ref}\,f(\xi,\eta;\kappa;V_o);\ \xi=\frac{y}{H}\ ;\ \eta=\frac{z}{H} \tag{26}$$

where P_{ref} is arbitrary since Eq. (25) is linear. The quantity 2H is the duct height (see Fig. 4). Substituting Eq. (26) into Eq. (25) the nondimensional wave equation is written

$$\frac{\partial^2 f}{\partial \xi^2}+\frac{\partial^2 f}{\partial \eta^2}+\frac{2\kappa}{(1-\kappa M_o)}\left[\left(\frac{\partial M_o}{\partial \xi}\right)\left(\frac{\partial f}{\partial \xi}\right)+\left(\frac{\partial M_o}{\partial \eta}\right)\left(\frac{\partial f}{\partial \eta}\right)\right]+(KH)^2\left[(1-\kappa M_o)^2-\kappa^2\right]f=0 \tag{27}$$

where $K\equiv\omega/c_o$.

4. PERTURBATION SOLUTION

A perturbation scheme to solve Eq. (27) is sought by expanding the eigenfunction f and eigenvalue κ in a power series of M_c, the mean flow center-line Mach number as follows

$$f(\xi,\eta;\kappa;V_o) = f_o(\xi,\eta;\kappa) + M_c f_1(\xi,\eta;\kappa) + M_c^2 f_2(\xi,\eta;\kappa)$$

$$+ \cdots = \sum_{i=0}^{\infty} M_c^{\,i} f_i(\xi,\eta;\kappa) \qquad (28)$$

$$\kappa(V_o) = \kappa_o + M_c \kappa_1 + M_c^2 \kappa_2 + \cdots$$

$$= \sum_{i=0}^{\infty} M_c^{\,i} \kappa_i \qquad (29)$$

Here the mean flow center line Mach number is defined as

$$M_c\left(\xi = \frac{W}{H}, \eta = 1\right) = \frac{V_o}{c_o}(y=W, z=H) \qquad (30)$$

The physical meaning of Eqs. (28) and (29) is straight-forward. The expansion procedure assumes that the effects of convection and refraction are small - sufficiently small so that the leading or dominant term is independent of the mean flow. This is the physical basis for the perturbation approach adopted.

4.1 Mean Flow Velocity Profile and Boundary Conditions

Before proceeding further, the mean flow velocity profile must be specified. The analysis will be restricted to ducts sufficiently long to establish fully-developed mean flow. Thus the mean flow boundary layer will be independent of the duct axial position. This means that the boundary-layer thicknesses in both the y and z direction will extend to the duct center defined in Fig. 4 as z=H and y=W. The rectangular duct geometry is such that the mean

flow is symmetrical in the y and z direction with respect to the duct center. With this understanding, the solution to Eqs. (28) and (29) will be derived only for the quadrant defined by $z \le H$ and $y \le W$.

The following fully-developed mean flow is proposed,

$$V_o(y,z) = V_c \left(\frac{y}{W}\right)^N \left(\frac{z}{H}\right)^N \tag{31}$$

where N is an arbitrary parameter that depends upon the flow Reynolds numbers $(V_c H/\nu)$ and/or $(V_c W/\nu)$, and V_c is the mean flow centerline value. For Reynolds numbers of the order of several million, representative of the usual kind of duct turbulence, N=1/7. In nondimensional terms, Eq. (31) is written

$$M(\xi,\eta) = M_c \left(\frac{H}{W}\right)^N \xi^N \eta^N \equiv M_c \beta^N \xi^N \eta^N \tag{32}$$

where $\beta \equiv H/W$ is the duct aspect ratio. Substituting Eqs. (28)-(32) into Eq. (27) and collecting coefficients of the powers of M_c yields to order M_c^2,

$$M_c^o \left\{ \frac{\partial^2 f_o}{\partial \xi^2} + \frac{\partial^2 f_o}{\partial \eta^2} + (KH)^2 (1-\kappa_o^2) f_o \right\} +$$

$$M_c \left\{ \frac{\partial^2 f_1}{\partial \xi^2} + \frac{\partial^2 f_1}{\partial \eta^2} + 2\kappa_o N \beta^N (\xi\eta)^{N-1} \left(\eta \frac{\partial f_o}{\partial \xi} + \xi \frac{\partial f_o}{\partial \eta}\right) \right.$$

$$\left. + (KH)^2 \left[(1-\kappa_o^2) f_1 + 2\beta^N (\xi\eta)^N \kappa_o f_o - 2\kappa_o \kappa_1 f_o \right] \right\} +$$

$$M_c^2 \left\{ \frac{\partial^2 f_2}{\partial \xi^2} + \frac{\partial^2 f_2}{\partial \eta^2} + 2\kappa_1 N \beta^N (\xi\eta)^{N-1} \left(\eta \frac{\partial f_0}{\partial \xi} + \xi \frac{\partial f_0}{\partial \eta} \right) \right.$$

$$+ 2\kappa_0^2 N \beta^{2N} (\xi\eta)^{2N-1} \left(\eta \frac{\partial f_0}{\partial \xi} + \xi \frac{\partial f_0}{\partial \eta} \right) + 2\kappa_0 N \beta^{N-1} (\xi\eta)^{N-1} \left(\eta \frac{\partial f_1}{\partial \xi} + \xi \frac{\partial f_1}{\partial \eta} \right)$$

$$+ (KH)^2 \left[(1-\kappa_0) f_2 - 2\kappa_0 \beta^N (\xi\eta)^N f_1 - 2\kappa_1 \beta^N (\xi\eta)^N f_0 - 2\kappa_0 \kappa_1 f_1 \right.$$

$$\left. \left. + \kappa_0^2 \beta^{2N} (\xi\eta)^{2N} f_0 - (\kappa_1^2 + 2\kappa_0 \kappa_2) f_0 \right] \right\} = 0 \qquad (33)$$

The first term in Eq. (33) is the classical wave equation governing the propagation of sound in a rectangular duct for *the case of zero grazing flow*. The solution is well-known and corresponds physically to the propagation of all the cut-on modes consistent with the source excitation frequency. Observe that the influence of the lower-order solutions act as nonhomogeneous source terms on the right-hand-side of the higher-ordered equations.

The governing sound propagation equations described by Eq. (33) must satisfy the rigid-wall boundary conditions of zero normal flow defined as,

$$v(x,0,z,t) = v(x,W,z,t) = w(x,y,0,t) = w(x,y,H,t) = 0 \qquad (34)$$

From Eqs. (23) and (24) this translates into the Neumann boundary conditions

$$\frac{\partial F}{\partial y}(0,z) = \frac{\partial F}{\partial y}(W,z) = \frac{\partial F}{\partial z}(y,0) = \frac{\partial F}{\partial z}(y,H) = 0 \qquad (35)$$

For the special case wherein the zero-ordered perturbation represents the plane-wave sound field, the leading terms of Eqs. (28) and (29) become

$$f_0(\xi,\eta) = \kappa_0 = 1 \tag{36}$$

In this case, Eq. (33) simplifies to

$$\frac{\partial^2 f_1}{\partial \xi^2} + \frac{\partial^2 f_1}{\partial \eta^2} = 2(KH)^2\left[(\beta\xi\eta)^N + \kappa_1\right] \tag{37}$$

and

$$\frac{\partial^2 f_2}{\partial \xi^2} + \frac{\partial^2 f_2}{\partial \eta^2} = -2N\beta^N(\xi\eta)^{N-1}\left[\eta\frac{\partial f_1}{\partial \xi} + \xi\frac{\partial f_1}{\partial \eta}\right]$$

$$+(KH)^2\left[2(\beta\xi\eta)^N(f_1+\kappa_1) - (\beta\xi\eta)^{2N} + (\kappa_1^2 + 2\kappa_2)\right] \tag{38}$$

4.2 General Solution

Equations (37) and (38) are the well known Poisson Equations subject to the Neumann boundary conditions defined by Eq. (35) Solutions to the functions $f_1(\xi,\eta)$ and $f_2(\xi,\eta)$ are sought by expanding them in a double Fourier series in terms of the homogeneous eigenfunctions $\cos(m\pi\beta\xi)\cos(\ell\pi\eta)$. The general solution to Eq. (37) will be formulated. First expand $f_1(\xi,\eta)$ as follows

$$f_1(\xi,\eta) = \sum_{m=0}^{\infty}\sum_{\ell=0}^{\infty} C_{m\ell}\cos(m\pi\beta\xi)\cos(\ell\pi\eta) =$$

$$A_{oo} + \sum_{m=1}^{\infty} A_m\cos(m\pi\beta\xi) + \sum_{\ell=1}^{\infty} B_\ell\cos(\ell\pi\eta) \qquad (39)$$

$$+ \sum_{m=1}^{\infty}\sum_{\ell=1}^{\infty} C_{m\ell}\cos(m\pi\beta\xi)\cos(\ell\pi\eta)$$

Next, expand the nonhomogeneous terms (RHS) of Eq. (37) in a similar manner

$$2(KH)^2\left[(\beta\xi\eta)^N + \kappa_1\right] = 2(KH)^2\kappa_1 + 2(KH)^2 G_{oo}$$

$$+ 2(KH)^2\sum_{m=1}^{\infty} G_m\cos(m\pi\beta\xi) + 2(KH)^2\sum_{\ell=1}^{\infty} H_\ell\cos(\ell\pi\eta)$$

$$+ 2(KH)^2\sum_{m=1}^{\infty}\sum_{\ell=1}^{\infty} I_{m\ell}\cos(m\pi\beta\xi)\cos(\ell\pi\eta) \qquad (40)$$

The coefficients A_{oo}, A_m, B_ℓ, $C_{m\ell}$, G_{oo}, G_m, H_ℓ and $I_{m\ell}$ are constants. The constants G_{oo}, G_m, H_ℓ and $I_{m\ell}$ are defined using standard Fourier analysis as

$$G_{oo} \equiv \beta\int_0^{1/\beta} d\xi\int_0^1 (\beta\xi\eta)^N\, d\eta = \frac{1}{(N+1)^2} \qquad (41)$$

$$G_m \equiv 2\beta\int_0^1\int_0^{1/\beta}(\beta\xi\eta)^N\cos(m\pi\beta\xi)\,d\xi\,d\eta = \frac{2\beta^{N+1}}{(N+1)}\,E_m \qquad (42)$$

where

$$E_m \equiv \int_0^{1/\beta} \xi^N \cos\left(m\pi\beta\xi\right) d\xi \tag{43}$$

In a similar manner, the coefficient H_ℓ may be evaluated as

$$H_\ell \equiv \left(\frac{2}{N+1}\right) J_\ell \tag{44}$$

where

$$J_\ell \equiv \int_0^1 \eta^N \cos\left(\ell\pi\eta\right) d\eta \tag{45}$$

The final coefficient $I_{m\ell}$ is

$$I_{m\ell} \equiv 4\beta \int_0^{1/\beta}\int_0^1 \left(\beta\xi\eta\right)^N \cos\left(m\pi\beta\xi\right)\cos\left(\ell\pi\eta\right) d\xi d\eta = 4\beta^{N+1} E_m J_\ell \tag{46}$$

The solution to Eq. (37) follows immediately upon connecting the coefficients A_{oo}, A_m, B_ℓ, $C_{m\ell}$ to the known coefficients G_{oo}, G_m, H_ℓ, $I_{m\ell}$. Substitution of Eq. (39) into Eq. (37) and collecting coefficients of the various cosine terms yields the following relations

$$A_m = \frac{-2(KH)^2 G_m}{m^2\pi^2\beta^2} \; ; \; B_\ell = \frac{-2(KH)^2 H_\ell}{\ell^2\pi^2} \; ; \; C_{m\ell} = \frac{-2(KH)^2 I_{m\ell}}{\pi^2\left(m^2\beta^2+\ell^2\right)} \tag{47}$$

The coefficient G_{oo} is determined by satisfying the compatibility relationship defined as

$$\beta \int_0^1 \int_0^{1/\beta} \mathcal{K}_1 \, d\xi \, d\eta = -G_{oo} = -\beta \int_0^1 \int_0^{1/\beta} (\beta\xi\eta)^N d\xi = -\frac{1}{(N+1)^2} \tag{48a}$$

Thus

$$\mathcal{K}_1 = -\frac{1}{(N+1)^2} \tag{48b}$$

Putting it all together, the first term perturbation solution is

$$f_1(\xi,\eta) = A_{oo} - \frac{4(KH)^2\beta^{N+1}}{(N+1)\pi^2} \sum_{m=1}^{\infty} \frac{E_m \cos(m\pi\beta\xi)}{m^2}$$

$$\frac{-4(KH)^2}{(N+1)\pi^2} \sum_{\ell=1}^{\infty} \frac{J_\ell \cos(\ell\pi\eta)}{\ell^2} - \frac{8(KH)^2\beta^{N+1}}{\pi^2} \sum_{m=1}^{\infty} \sum_{\ell=1}^{\infty} \frac{E_m J_\ell \cos(m\pi\beta\xi)\cos(\ell\pi\eta)}{(m^2\beta^2+\ell^2)} \tag{49}$$

The coefficient A_{oo} in Eq. (49) is arbitrary for the Neumann problem. The following tentative physical interpretation is offered. A nonzero value could be interpreted as a source of acoustic energy. The idea here is based on Morfey's[16] study of production of acoustic energy in a flow duct/sound system from interaction between the sound field and the mean flow vorticity (JSV: Vol 14, 159-170, 1971). Morfey showed that sound can be generated (or absorbed) by the mean flow providing the mean flow is (1) vortical and (2) three-dimensional. Both conditions are satisfed in the present case. *Since it is beyond the scope of this study to consider the production of acoustic energy, it will be assumed herein that the sole effect of the mean shear flow is to redistribute acoustic pressure.* Thus it follows that the plane wave pressure, normalized to unity, must satisfy the constraint that

$$\int_0^{1/\beta}\int_0^{1} p(\xi,\eta)\,d\xi\,d\eta = 1 \rightarrow \int_0^{1/\beta}\int_0^{1} f_i(\xi,\eta)\,d\xi\,d\eta = 0 \qquad (50)$$

for all i.

5. SOLUTION FOR THE CASE N=1

A detailed solution to second order for the case N=1 is presented for a linear mean flow velocity profile. The advantage of the linear velocity gradient case (N=1) is that Eqs. (43), (44) and (45) can be easily integrated to yield analytic expressions for the perturbation solutions of $f_1(\xi,\eta)$ and $f_2(\xi,\eta)$. For this flow, the refraction effect of the shear flow (e.g., $\partial V_0/\partial\xi \sim N$) is larger for this case than for, say, the N=1/7 velocity profile. To further simplify the analysis, the duct cross-section will be square so that $\beta \equiv H/W = 1$ (this shape corresponds to the Langley flow duct facility).

5.1 First-Order Solution

Substituting N=1 into Eqs. (43), (44) and (45) and evaluating the integrals yields

$$E_m = -\frac{1}{(m\pi)^2}\left[1-(-1)^m\right] = \frac{-2}{\pi^2(2m-1)^2} \qquad (51)$$

$$H_\ell = -\frac{1}{(\ell\pi)^2}\left[1-(-1)^\ell\right] = \frac{-2}{\pi^2(2\ell-1)^2} \qquad (52)$$

$$I_{m\ell} = \frac{4}{\pi^4 m^2 \ell^2}\left[1-(-1)^m\right]\left[1-(-1)^\ell\right] = \frac{16}{\pi^4(2m-1)^2(2\ell-1)^2} \qquad (53)$$

Substituting these values into Eq. (49) results in the following solution to $f_1(\xi,\eta)$,

$$f_1(\xi,\eta) = A_{oo} + \frac{4(KH)^2}{\pi^4}\sum_{m=1}^{\infty}\frac{\cos[(2m-1)\pi\xi]}{m^2(2m-1)^2} + \frac{4(KH)^2}{\pi^4}\sum_{\ell=1}^{\infty}\frac{\cos[(2\ell-1)\pi\eta]}{\ell^2(2\ell-1)^2}$$

$$- \frac{32(KH)^2}{\pi^6}\sum_{m=1}^{\infty}\sum_{\ell=1}^{\infty}\frac{\cos(m\pi\xi)\cos(\ell\pi\eta)}{(2m-1)^2(2\ell-1)^2(m^2+\ell^2)} \qquad (54)$$

Equation (54) is exact. It is clear that it satisfies the boundary conditions

$$\frac{\partial f_1}{\partial \xi}(0,\eta) = \frac{\partial f_1}{\partial \xi}(1,\eta) = \frac{\partial f_1}{\partial \eta}(\xi,0) = \frac{\partial f_1}{\partial \eta}(\xi,1) = 0 \qquad (55)$$

In order to satisfy the constraint imposed by Eq. (50) that the mean flow vorticity does not act as a source (or sink) of acoustic energy production, it is straight-forward to show that $A_{oo}=0$ in Eq. (54). With $A_{oo}=0$, Eq. (54) is shown graphically in Fig. 5. The symbols shown in Figure 5 represent the solution Eq. (54) calculated to within one percent accuracy. The dashed lines represent the following curve fit,

$$f_1(\xi,\eta) \simeq (KH)^2\left\{.021 + .042\cos^2\left(\frac{\pi\xi}{2}\right)\cos^2\left(\frac{\pi\eta}{2}\right)\right.$$
$$\left. - (.339 + .016\xi)(.339 + .016\eta)\sin^2\left(\frac{\pi\xi}{2}\right)\sin^2\left(\frac{\pi\eta}{2}\right)\right\} \qquad (56)$$

As an independent check on the accuracy of the above curve fit to $f_1(\xi,\eta)$, it satisfies the energy constraint Eq. (50), to the following accuracy

$$\int_0^1\int_0^1 f_1(\xi,\eta)\,d\xi\,d\eta = 5.4 \times 10^{-5} \tag{57}$$

The purpose of the above curve fit is to simplify enormously the calculations required to compute the second-ordered perturbation solution $f_2(\xi,\eta)$. The curve fit is sufficiently accurate to represent both the function $f_1(\xi,\eta)$ and its first derivatives $\partial f_1/\partial\xi$ and $\partial f_1/\partial\eta$ both of which are required to calculate $f_2(\xi,\eta)$ as shown in Eq. (38). It is clear from Fig. 5 that the effect of the shear flow is to redistribute the initially plane wave acoustic pressure in such a way as to increase (decrease) the local pressure near the wall for downstream (upstream) sound propagation (i.e., near $\xi = 0$ and $\eta = 0$) relative to its value at the duct center ($\xi=\eta=1$). From Eq. (48) the eigenvalue

$$\kappa_1 = -\frac{1}{4} \tag{58}$$

Further physical interpretation is deferred until the solution to $f_2(\xi,\eta)$ is obtained.

5.2 Second-Order Solution

The solution to the second-order pressure $f_2(\xi,\eta)$ perturbation is similar to that used to calculate $f_1(\xi,\eta)$. Substituting $N=\beta=1$ into Eq. (38) results in the following Poisson equation

$$\frac{\partial^2 f_2}{\partial\xi^2} + \frac{\partial^2 f_2}{\partial\eta^2} = -2\eta\frac{\partial f_1}{\partial\xi} - 2\xi\frac{\partial f_1}{\partial\eta} + (KH)^2\left[\left(2\xi\eta-\tfrac{1}{2}\right)f_1 - \tfrac{1}{2}\xi\eta - (\xi\eta)^2 + \left(\tfrac{1}{16}+2\kappa_2\right)\right] \tag{59}$$

The eigenvalue κ_2 is completed from the RHS of Eq. (59) by imposing the compataiblity relation that

$$\int_0^1 \int_0^1 (RHS)\, d\xi\, d\eta = 0 \tag{60}$$

Substituting Eq. (56) into Eq. (59) and integrating results in the following approximate expression for κ_2,

$$\kappa_2 \simeq -.015 + .009\,(KH)^2 \tag{61}$$

Thus an approximate solution to the effects of refraction on the axial propagation of the plane wave, valid to second-order, is

$$\kappa \simeq 1 - \frac{M_c}{4} - M_c^2 \left[.015 - .009\,(KH)^2 \right] \tag{62}$$

Referring back to Eqs. (4)-(6), the eigenvalue κ is related to the propagation speed of the sound energy - that is, the group speed (V_g). Recall that for sound propagation through a dispersive media, the group speed is a measure of the average rate of transport of acoustic energy. Its mathematical definition is

$$V_g = \frac{\partial \omega}{\partial K_x} \tag{63}$$

where

$$K_x = \frac{\omega}{C_o}\,\kappa \simeq \frac{\omega}{C_o} \left\{ 1 - \frac{M_c}{4} - M_c^2 \left[.015 - .009 (KH)^2 \right] \right\} \tag{64}$$

Performing the necessary differentiation, the group speed, normalized to the local sound speed c_o, is approximately

$$M_g \equiv \frac{V_g}{c_o} = \frac{1}{1 - \frac{M_c}{4} - M_c^2 \left[.015 - .018 \left(\frac{\omega H}{c_o} \right)^2 \right]} \tag{65}$$

Figure 6 shows a comparison between the group velocity defined by Eq. (65) and the group velocity corresponding to the propagation of plane wave sound in a uniform mean flow. It is well known that for sound propagation in a uniform mean flow, the group velocity is equivalent to the sound wave phase speed. Thus

$$\frac{V_g}{c_o} = \frac{V_p}{c_o} = 1 + M_c \tag{66}$$

Figure 6 shows that the group speed for the shear flow case is quite insensitive to the centerline mean flow speed in contrast to the uniform flow case. The effects of refraction appear to focus the group velocity to values near c_o for both upstream and downstream sound propagation.

With $\mathcal{K}_2$ specified, the RHS of Eq. (59) is known. Its solution follows exactly the procedure described above in Section 5.1. Substituting Eq. (56) for $f_1(\xi, \eta)$ into the RHS of Eq. (59) results in the following rather complicated Poisson Equation,

$$\frac{\partial^2 f_2}{\partial \xi^2} + \frac{\partial^2 f_2}{\partial \eta^2} = (KH)^2 \left\{ \pi \eta \sin(\pi \xi) \left[.042 \cos^2 \left(\frac{\pi \eta}{2} \right) \right. \right.$$

$$\left. + (.339 + .016\xi)(.339 + .016\eta) \sin^2 \left(\frac{\pi \eta}{2} \right) \right] + .032 \sin^2 \left(\frac{\pi \xi}{2} \right) \sin^2 \left(\frac{\pi \eta}{2} \right) \left[(.339 + .016\xi)\xi + \right.$$

$$+ (.339 + .016\,\eta)\,\eta\Big] + \pi\xi \sin(\pi\eta)\Big[.042 \cos^2\left(\frac{\pi\xi}{2}\right) +$$

$$(.339 + .016\,\xi)(.339 + .016\,\eta)\sin^2\left(\frac{\pi\eta}{2}\right)\Big] + \Big[.033 - \frac{1}{2}(\xi\eta) - (\xi\eta)^2\Big] \Bigg\}$$

$$+ (KH)^4 \Bigg\{ .018 + (2\xi\eta - \tfrac{1}{2})\Big[.021 + .042 \cos^2\left(\frac{\pi\xi}{2}\right)\cos^2\left(\frac{\pi\eta}{2}\right)$$

$$- (.339 + .016\,\xi)(.339 + .016\,\eta)\sin^2\left(\frac{\pi\xi}{2}\right)\sin^2\left(\frac{\pi\eta}{2}\right)\Big]\Bigg\} \equiv (KH)^2 \cdot A(\xi,\eta)$$

$$+ (KH)^4 \cdot B(\xi,\eta) \tag{67}$$

Obviously, the RHS of Eq. (67) is quite complicated. To reduce the computational calculations, it has been simplified as shown in Figures 7 and 8 to the following curve fit expressions for $A(\xi,\eta)$ and $B(\xi,\eta)$,

$$A(\xi,\eta) \simeq .033 + (\xi\eta)\Big[.673 - 1.583\,(\xi\eta) - .567\,(\xi\eta)^2\Big] \tag{68}$$

$$B(\xi,\eta) \simeq -.015 + (\xi\eta)\Big[.097 - .256\,(\xi\eta)\Big] + .021\,(\xi+\eta) \tag{69}$$

As a check on the accuracy of Eqs. (68) and (69), the compatibility relationship requires that the integral of the RHS of Eq. (67) vanish yielding

$$\int_0^1\int_0^1 \Big[(KH)^2 A(\xi,\eta) + (KH)^4 B(\xi,\eta)\Big]\,d\xi\,d\eta = .01(KH)^2 - .003(KH)^4 \tag{70}$$

The RHS of Eq. (70) is sufficiently close to zero to verify the accuracy of the curve fits defined by Eqs. (68) and (69). Using these equations and following the approach used in Section 5.1 above to evaluate the Fourier coefficients to the first perturbation pressure solution, the solution to the second perturbation pressure $f_2(\xi,\eta)$ is

$$
\begin{aligned}
f_2(\xi,\eta) \simeq \frac{(KH)^2}{\pi^4}\Bigg\{ & \sum_{m=1}^{\infty}\left[\frac{1.346}{m^2(2m-1)^2}+\frac{1.906(-1)^m}{m^4}+\frac{3.402}{\pi^2 m^2(2m-1)^2}\right]\cos(m\pi\xi) \\
& +\sum_{l=1}^{\infty}\left[\frac{1.346}{l^2(2l-1)^2}+\frac{1.906(-1)^l}{l^4}+\frac{3.402}{\pi^2 l^2(2l-1)^2}\right]\cos(l\pi\eta) \\
& +\sum_{m=1}^{\infty}\sum_{l=1}^{\infty}\Bigg[\frac{-10.77}{(2m-1)^2(2l-1)^2(m^2+l^2)\pi^2}+\frac{45.74\,(-1)^{m+l}}{m^2l^2(m^2+l^2)\pi^2} \\
& +\frac{81.65}{l^2(2m-1)^4(m^2+l^2)\pi^4}+\frac{81.65}{m^2(2l-1)^4(m^2+l^2)\pi^4}+\frac{326.59}{(2m-1)^4(2l-1)^2(m^2+l^2)\pi^6}\Bigg]\cos(m\pi\xi)\cos(l\pi\eta)\Bigg\} \\
+\frac{(KH)^4}{\pi^6}\Bigg\{ & \sum_{m=1}^{\infty}\left[\frac{.276}{m^2(2m-1)}+\frac{.167(-1)^m}{m^4}\right]\cos(m\pi\xi)+ \\
& \sum_{l=1}^{\infty}\left[\frac{.276}{l^2(2l+1)^2}+\frac{.167(-1)^l}{l^4}\right]\cos(l\pi\eta)+ \\
& \sum_{m=1}^{\infty}\sum_{l=1}^{\infty}\left[\frac{-1.555}{(2m-1)^2(2l-1)^2(m^2+l^2)}+\frac{4.099(-1)^{m+l}}{m^2l^2(m^2+l^2)}\right]\cos(m\pi\xi)\cos(l\pi\eta)\Bigg\}
\end{aligned}
\tag{71}
$$

Equation (71) is rewritten in the more convenient form with one term proportional to $(KH)^2$ and a second proportional to $(KH)^4$,

$$f_2(\xi,\eta) \simeq (KH)^2 C(\xi,\eta) + (KH)^4 D(\xi,\eta) \tag{72}$$

The coefficients and approximate curve fits to $C(\xi,\eta)$ and $D(\xi,\eta)$ are shown graphically in Figs. 9 and 10. The symbols represent numerical solutions to Eq. (71) and the dashed and continuous lines represent the following curve fits,

$$C(\xi,\eta) \simeq .024 \cos(\pi\xi)\cos(\pi\eta) + .018(\xi\eta)^3 \tag{73a}$$

$$\begin{aligned} D(\xi,\eta) \simeq\ & .001 \cos(\pi\xi)\cos(\pi\eta) + .0015 \sin(\pi\xi)\sin(\pi\eta) \\ & -.02(\xi\eta)(1.2-\xi)(1.2-\eta) + .0043(1-\xi)(1-\eta) - .0018(1-\xi)^2(1-\eta)^2 \end{aligned} \tag{73b}$$

Equations (73a) and (73b) satisfy the constraint of zero energy transfer between the mean vortical flow and the sound field. The integrals of the curve fits, Eqs. (72) and (73), are

$$\int_0^1\int_0^1 f_2(\xi,\eta)\,d\xi\,d\eta \simeq .001(KH)^2 - .0008(KH)^4 \tag{74}$$

which approximate zero sufficiently accurately. Thus the free constant equivalent to A_{oo} in Section .1 above is set equal to zero.

Combining Eqs. (28), (36), (56), (72), (73) and (74) results in the following approximate solution to second-order, for the sound pressure

$$\frac{F(y,z)}{P_{ref}} \simeq 1 + (KH)^2 M_c \left[.021 + .042 \cos^2\left(\frac{\pi y}{2H}\right) \cos^2\left(\frac{\pi z}{2H}\right) \right.$$

$$\left. - \left(.339 + .016 \frac{y}{H}\right)\left(.339 + .016 \frac{z}{H}\right) \sin^2\left(\frac{\pi y}{2H}\right) \sin^2\left(\frac{\pi z}{2H}\right) \right]$$

$$+ (KH)^2 M_c^2 \left[.024 \cos\left(\frac{\pi y}{H}\right) \cos\left(\frac{\pi z}{H}\right) + .018 \left(\frac{yz}{H^2}\right)^3 \right]$$

$$+ (KH)^4 M_c^4 \left[.001 \cos\left(\frac{\pi y}{H}\right) \cos\left(\frac{\pi z}{H}\right) + .0015 \sin\left(\frac{\pi y}{H}\right) \sin\left(\frac{\pi z}{H}\right) \right.$$

$$- .02 \left(\frac{yz}{H^2}\right)\left(1.2 - \frac{y}{H}\right)\left(1.2 - \frac{z}{H}\right) + .0043 \left(1 - \frac{y}{H}\right)\left(1 - \frac{z}{H}\right)$$

$$\left. - .0018 \left(1 - \frac{y}{H}\right)^2 \left(1 - \frac{z}{H}\right)^2 \right] \qquad (75)$$

Here P_{ref} is an arbitrary source strength. Equation (75) is only approximately correct - but is is sufficiently accurate to demonstrate the importance of the effects of refraction by the mean flow. Figure 11 shows the acoustic pressure distribution across the duct for the case KH=1 and Mc=0.2. The refraction effects are quite small. Figure 11 suggests that the ratio of the acoustic pressure at the origin y=z=0 to its value at the duct center y=z=H($\zeta = \eta = 1$) is a good measure of the distortion of the plane wave due to the mean flow refraction. From Eq. (75),

$$\frac{P_{oo}}{P_{11}} = \frac{1 + M_c\left[.063(KH)^2\right] + M_c^2\left[.024(KH)^2 + .0035(KH)^4\right]}{1 + M_c\left[-.105(KH)^2\right] + M_c^2\left[.018(KH)^2 + .0007(KH)^4\right]} \qquad (76)$$

Figure 12 summarizes Eq. (76) for a wide range of mean flow center Mach numbers and sound frequencies. It is clear that for low speed flow and for sound frequencies below the first mode cut-on frequency (corresponding to a axial wave number value $KH<\pi/2$), the effects of mean flow refraction are on the order of 1dB or less. For application to the Langley SWT duct flow facility, clearly the effects of refraction are unimportant. For downstream sound propagation, Fig.17 shows the effects of the mean flow is to refract the sound into the duct walls. For the upstream case, the sound is refracted into the duct center.

It is implicit in the formulation of the perturbation scheme described by Eqs. (28) and (29) , that both M_c and KH must be small in some "sense". The frequency parameter KH is straight-forward. For perturbations about plane-waves, $KH<\pi/2$. The range of validity of the centerline Mach number is defined in terms of convergence of Eqs. (28) and (29). From Eq. (78), it is clear that the maximum value of M_c for which Eq. (78) is valid is related directly to the value of (KH). Thus, M_c can be larger for smaller values of (KH). Consider for example, the numerator of Eq. (78) . For P_{oo} to be valid, the following two constraints must be met,

$$.063\,(KH)^2 M_c < 1 \tag{79}$$

$$(KH)^2 M_c{}^2 \left[.024 + .0035\,(KH)^2 \right] < .063\,(KH)^2 M_c \tag{80}$$

In general, the $m^{th}{}_{+1}$ term must be smaller than the m^{th} term. Equations (79) and (80) show that for $KH<\pi/2$, all subsonic center duct flow Mach number values are permissible.

6. CONCLUDING REMARKS

The perturbation model shows clearly that for low speed mean flows and for sound frequencies corresponding to plane-wave excitation, the mean flow velocity gradients only negligible distort the plane wave transverse pressure distribution across the duct. This conclusion is conservative in the sense that for mean velocity profiles defined by Eq. (32), the velocity gradient (vorticity) in either the y or z direction is proportional to N; thus selecting N=1 results in a much larger value of vorticity than the usual turbulent value of N=1/7. It is important to remind the reader that the above conclusion has been verified only for perturbation about the *plane-wave case*. An important finding of this study is that the effects of refraction do not significantly affect the standing wave pattern in a wave guide. This is valid providing the flow speed is low and only plane wave motion is excited within the waveguide.

A rather interesting result of this study is that the mean flow velocity gradients seems to focus the propagation of acoustic energy into a narrow window around the undisturbed adiabatic sound speed, both for upstream and downstream propagation. This is in contrast to the uniform mean flow sound energy propagation speed of $c_o(1+M_o)$, which is a strong function of the mean flow velocity.

Another interesting result is that the perturbation techniques permits the possibility of allowing for the production (or absorption) of acoustic energy through interaction between the mean (vortical) flow and the sound field. To consider this, however, the energy conservation equation must be studied using the technique described by Morfey.

REFERENCES

1. B. Phillips, "Effects of High Value Wave Amplitude and Mean Flow on a Helmholtz Resonator", NASA TMX-1582 (May 1968)

2. G. D. Garrison, et. al., "Suppression of Combustion Oscillations with Mechanical Damping Devices, Interim Report" PWA FR-3299 (Aug 1969)

3. J. S. Binek, "Behavior of Acoustic Resistance of Typical Duct Liners in the Presence of Grazing Flow Measured by the Two-Microphone Method", M.S. Thesis, Unviersity of Southampton (Oct. 1969)

4. P. D. Dean, "An In Situ Method of Wall Acoustic Impedance Measurements in Flow Ducts", J. Sound Vib., 34, No. 1, 97-130 (1974)

5. H. E. Plumblee Jr., P. D. Dean, G. A. Wynne and R. H. Burrin, "Sound Propagation in and Radiation from Acoustically Lined Flow Ducts - A Comparison of Experiment and Theory", NASA CR-2306 (Oct 1973)

6. A. S. Hersh and B. W. Walker, "The Acoustic Behavior of Helmholtz Resonators Exposed to High Speed Grazing Flows", AIAA Paper No. 76-536, AIAA 3rd AeroAcoustic Conference, Palo Alto, Calif., (July 1976)

7. E. Feder and L. W. Dean, "Analytical and Experimental Studies for Predicting Noise Attenuation in Acoustically Treated Ducts for Turbo Fan Engines", NASA CR-1373 (1969)

8. D. L. Armstrong, "Acoustic Grazing Flow Impedance Using Waveguide Principles", NASA CR-120848 (Dec 1972)

9. A. S. Hersh and I. Catton, "Effect of Shear Flow on Sound Propagation in Rectangular Ducts", Journ. of Acoustical Soc. Am., Vol 50, No. 3, Pt. 2, 992-1003 (Sept 1971)

10. A. H. Nayfeh, J. E. Kaiser, and D. P. Telion's, "Acoustics of Aircraft Engine-Duct Systems", AIAA Journal, Vol. 13, No. 2, 130-153, (Feb 1975)

11. D. C. Pridmore-Brown, "Sound Propagation in a Fluid Flowing Through an Attenuating Duct", Journal of Fluid Mechanics, Vol. 4, 393-406 (Aug 1958)

12. P. Mungur and G.M.L. Gladwell, "Acoustic Wave Propagation in a Sheared Fluid Contained in a Duct", Journal Sound Vibration, Vol. 9, No. 1, 28-48 (1969)

13. F. Mechel, P. Mertens, and W. Schilz, "Research on Sound Propagation in Sound-Absorbent Ducts with Superimposed Air Streams", Wright-Patterson Air Force Base, Ohio, AMRL Rep. TDR-62-140 (III) (Dec 1962)

14. D. H. Tack and R. F. Lambert, "Influence of Shear Flow in Sound Attenuation in Lined Ducts", J. Acoust. Soc. Amer. Vol. 38, No. 4 655-666 (1965)

15. P. Mungur and H. E. Plumblee, "Propagation and Attenuation of Sound in a Soft-Walled Annular Duct Containing a Sheared Flow", Presented at the NASA Basic Noise Res. Conf. (July 1969)

16. C. L. Morfey, "Acoustical Energy in Nonuniform Flows", J. Sound Vib, Vol. 14(2), 159-170, 1971

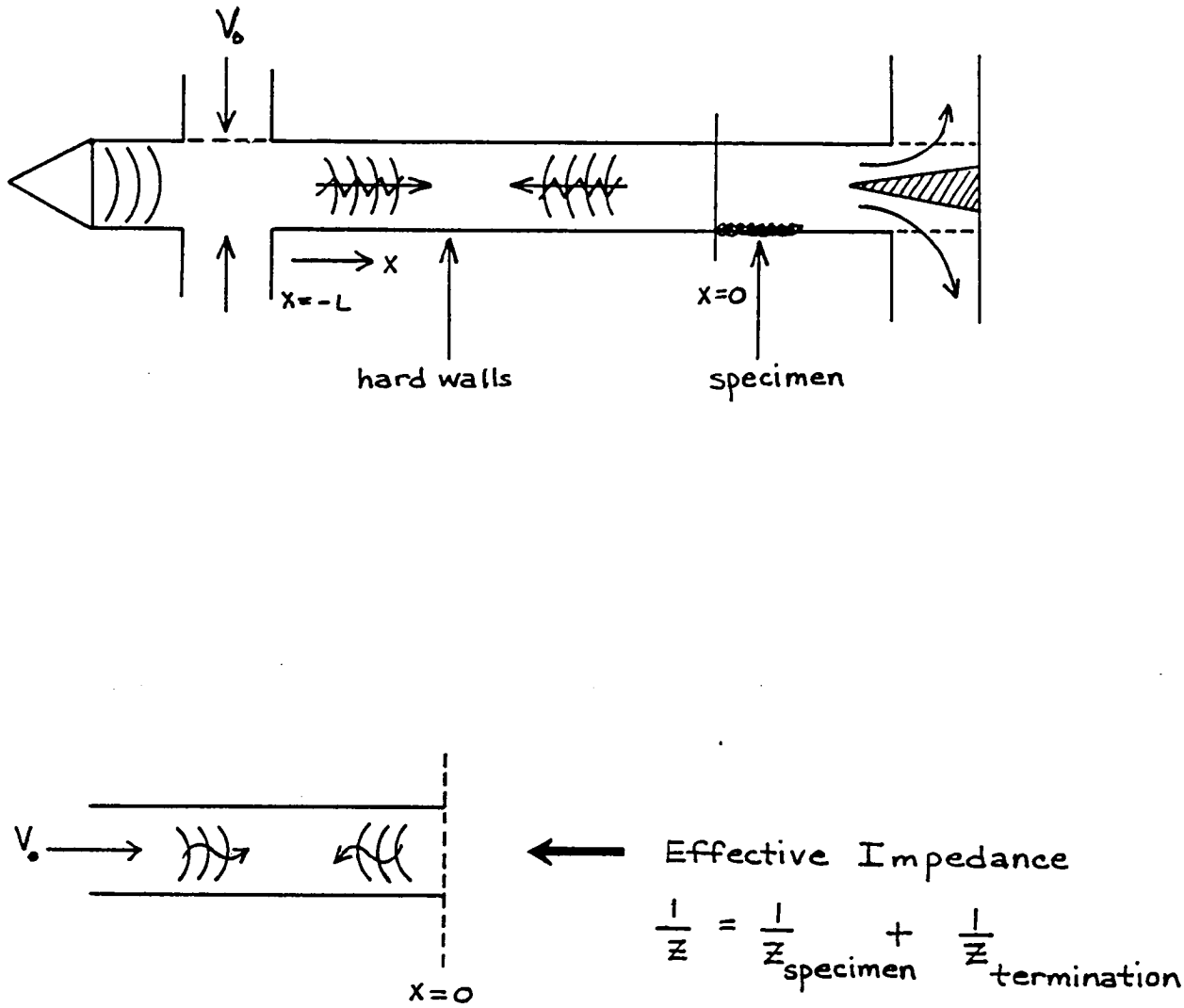

Figure 1. Schematic of SWT Impedance Model

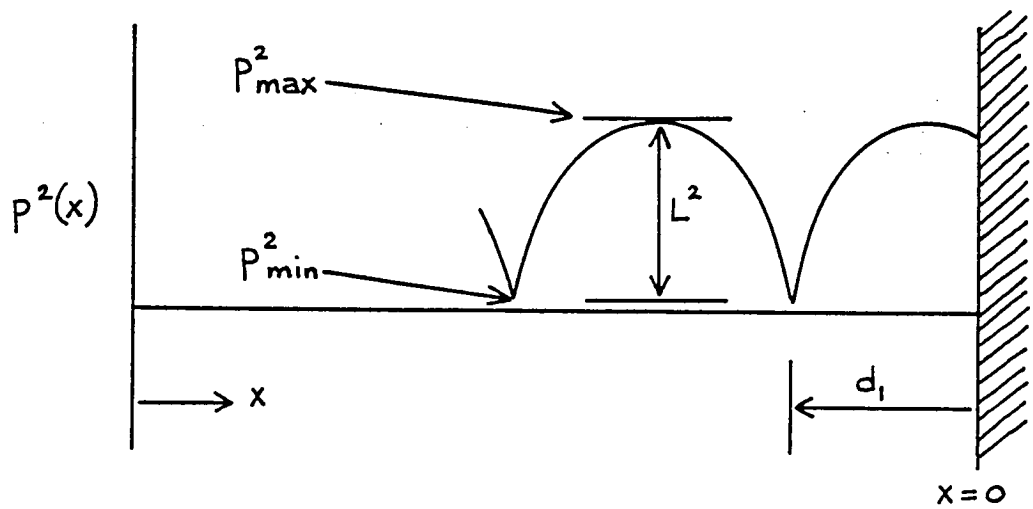

Figure 2. Connection Between SWT Pressure Distribution and Tube Geometry

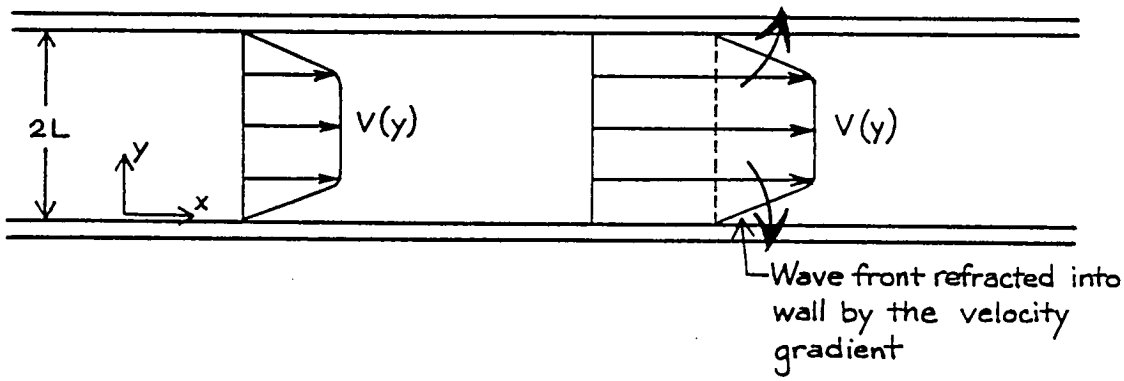

FIGURE 3a. SCHEMATIC OF DOWNSTREAM SOUND PROPAGATION

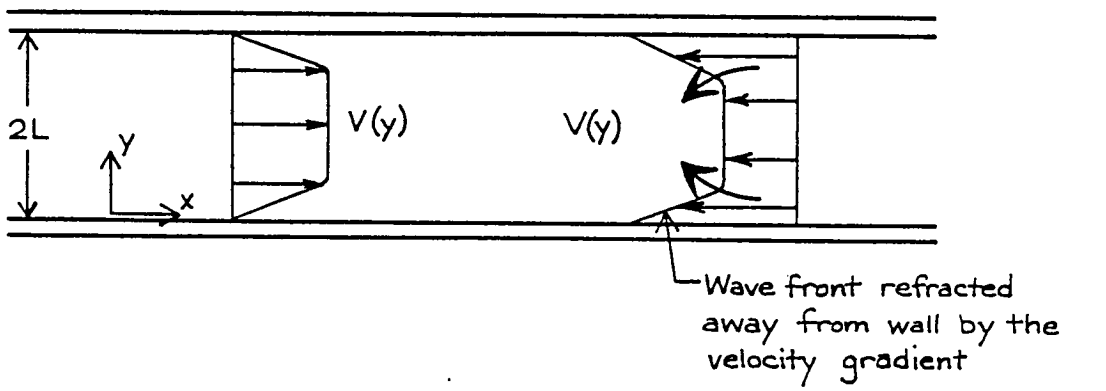

FIGURE 3b. SCHEMATIC OF UPSTREAM SOUND PROPAGATION

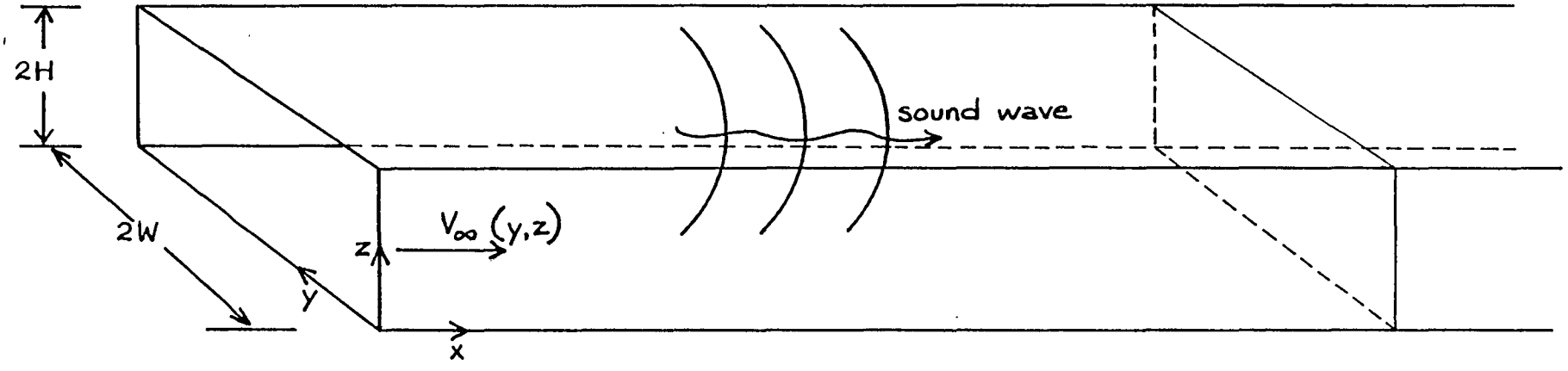

FIGURE 4. SCHEMATIC OF PLANE-WAVE PROPAGATION IN RECTANGULAR DUCT

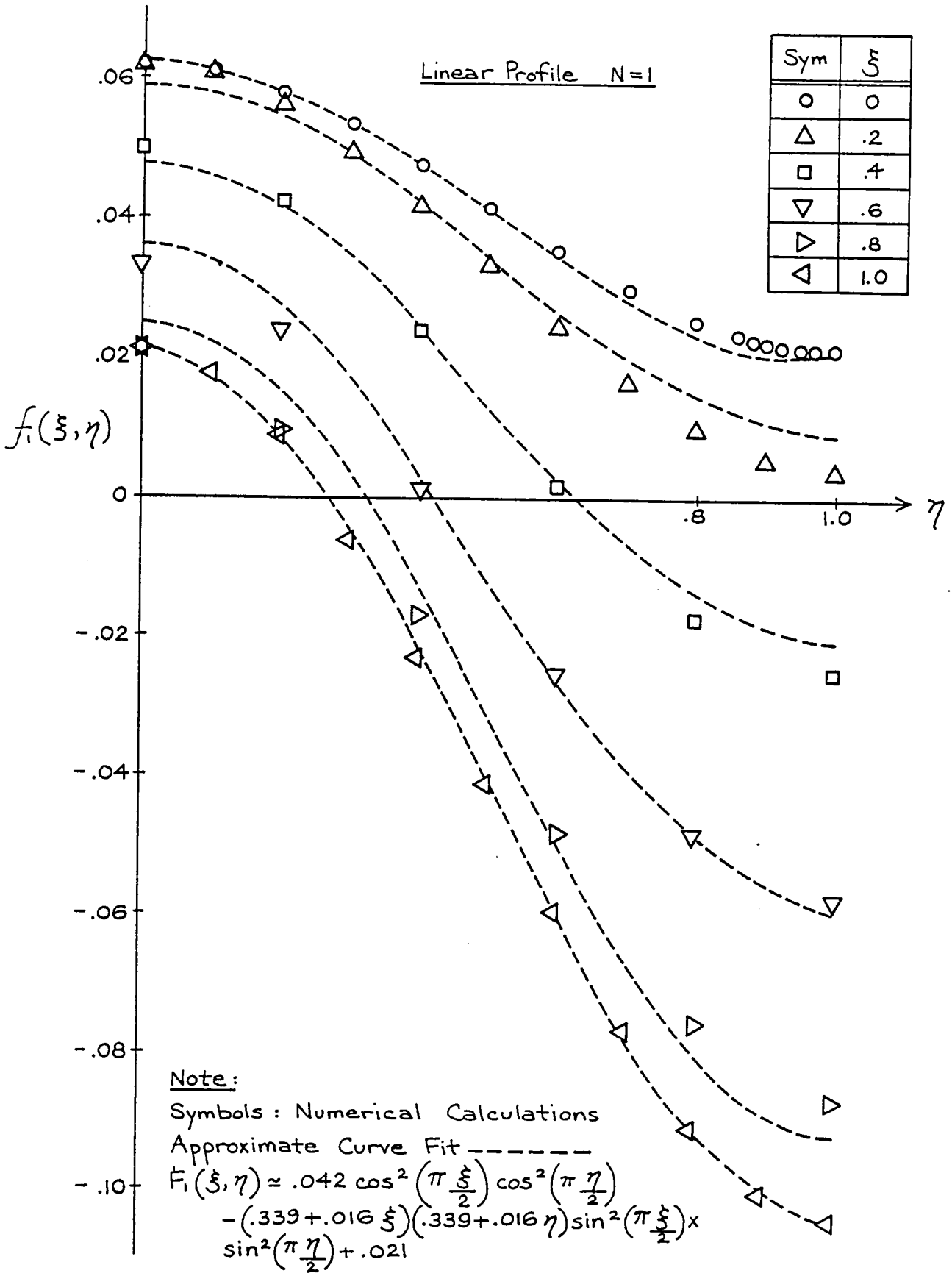

FIGURE 5. CURVE FIT OF FIRST PERTURBED ACOUSTIC PRESSURE

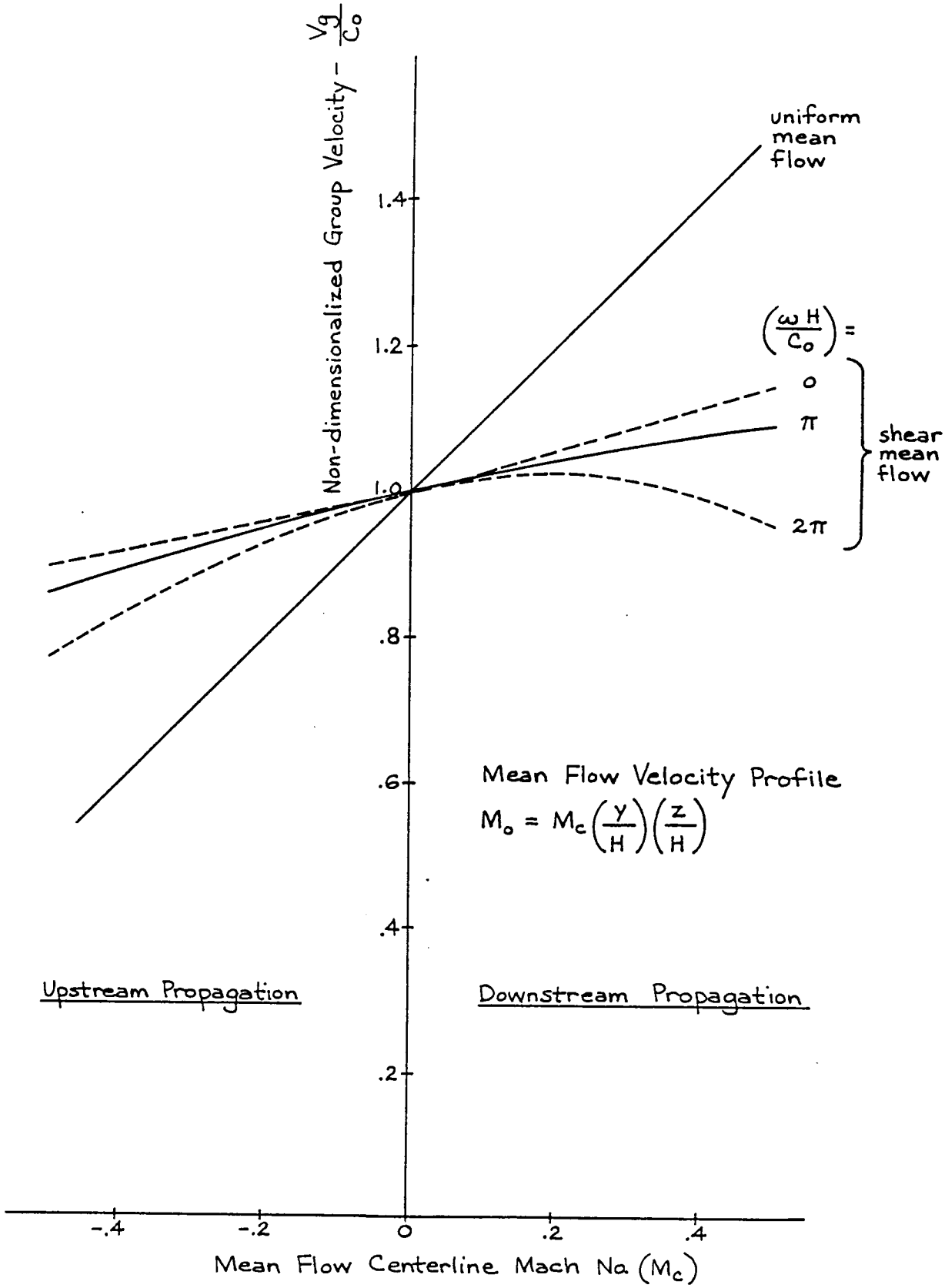

FIGURE 6. EFFECT OF MEAN FLOW ON PLANE-WAVE GROUP VELOCITY

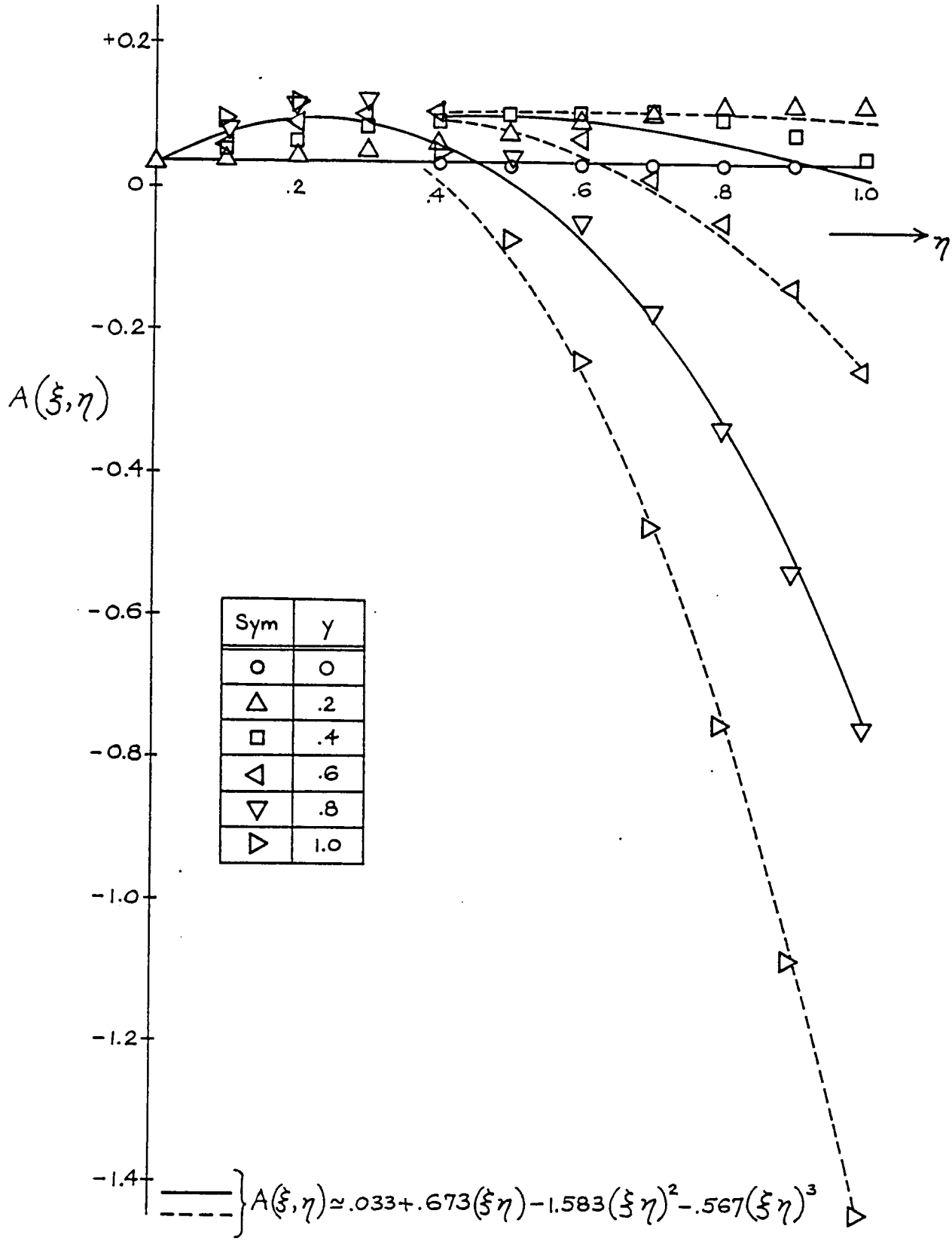

FIGURE 7. CURVE-FIT TO THE TERM PROPORTIONAL TO $(KH)^2$ ON THE RHS OF EQ. (67)

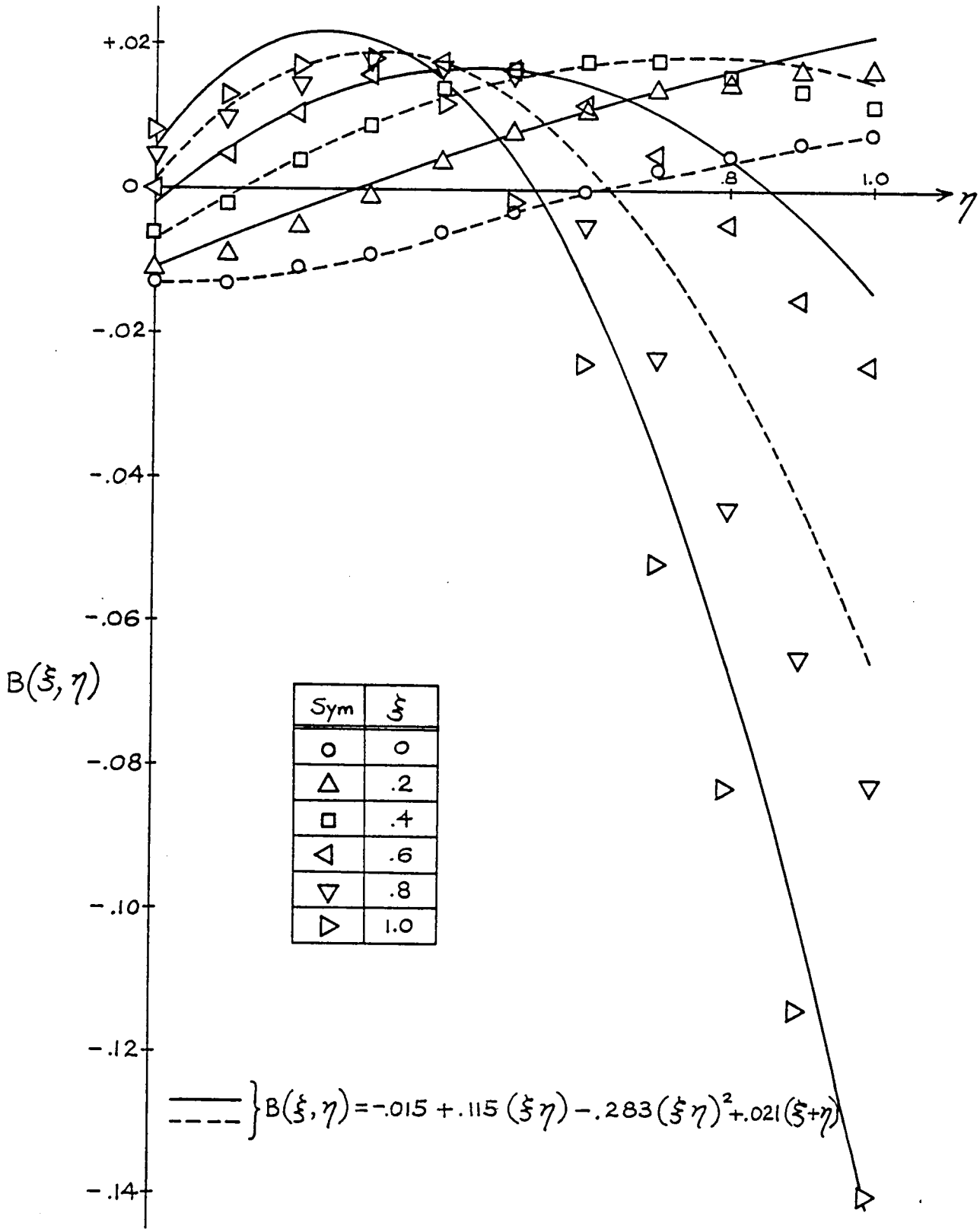

FIGURE 8. CURVE-FIT TO THE TERM PROPORTIONAL TO $(KH)^4$ ON THE RHS OF EQ. (67)

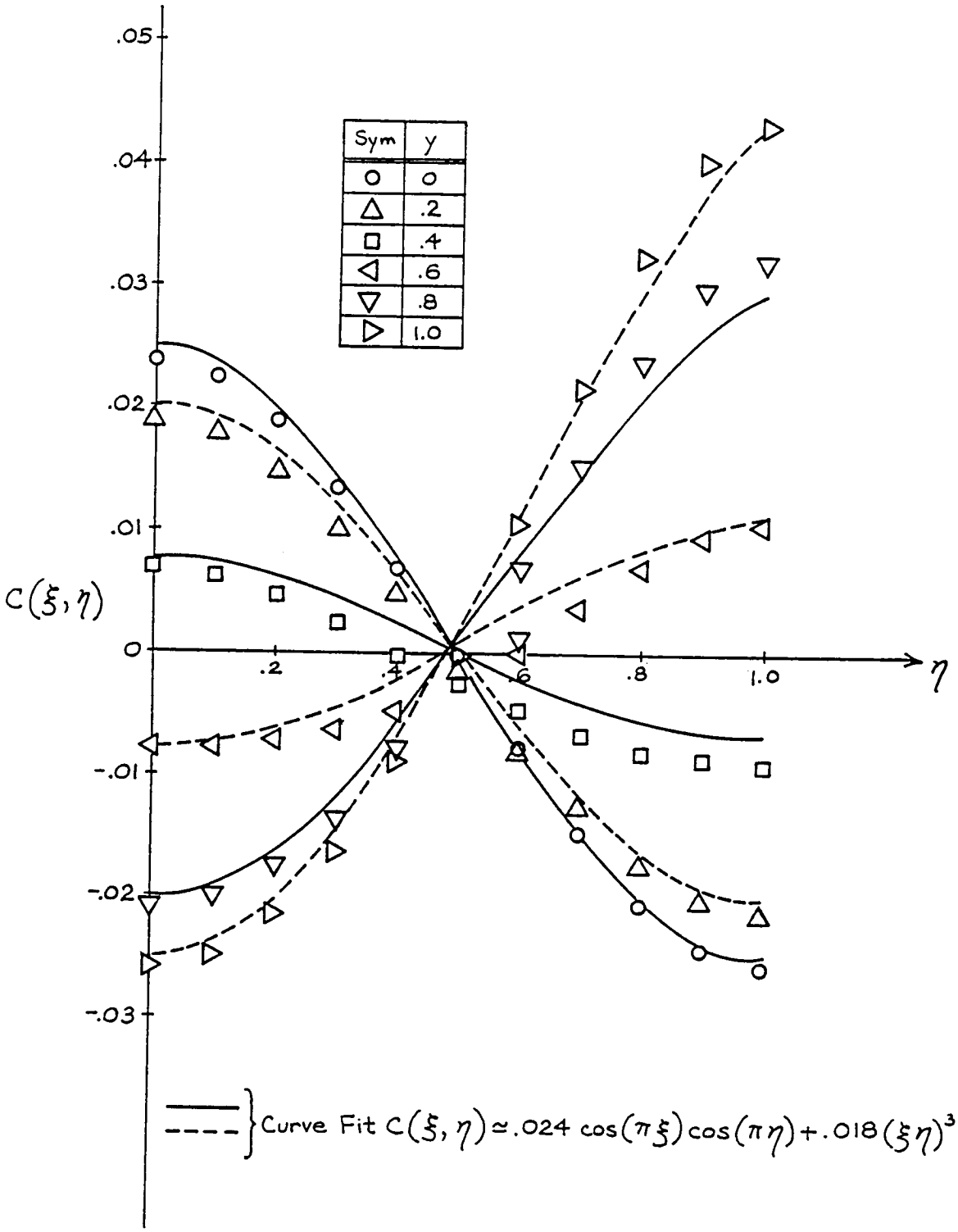

FIGURE 9. CURVE-FIT TO THE TERM PROPORTIONAL TO $(KH)^2$ ON THE RHS OF EQ. (71)

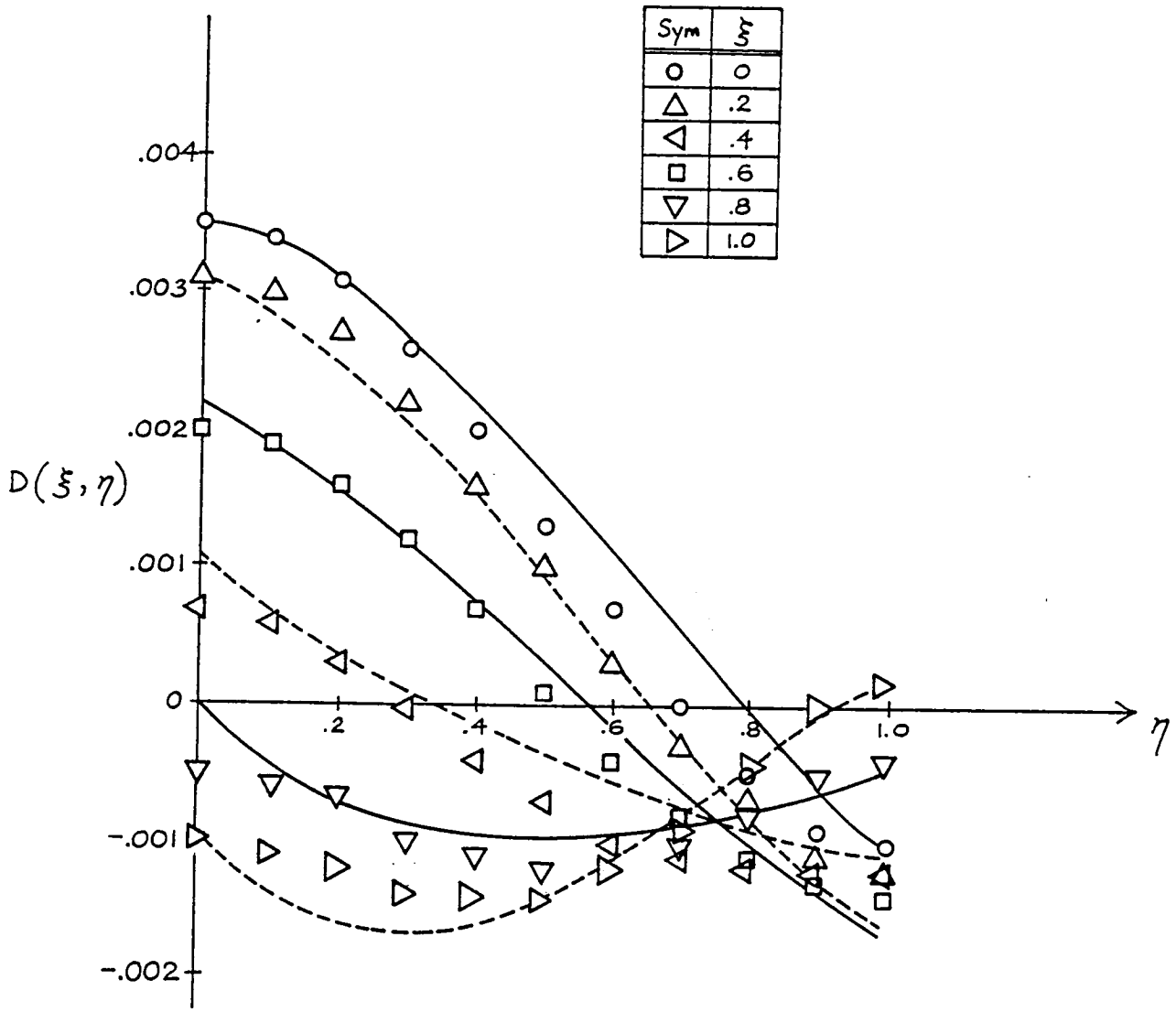

$$D(\xi,\eta) \simeq .001\cos(\pi\xi)\cos(\pi\eta) + .0015\sin(\pi\xi)\sin(\pi\eta) - .02\,\xi\eta(1.2-\xi)(1.2-\eta) + .0043(1-\xi)(1-\eta) - .0018(1-\xi)^2(1-\eta)^2$$

FIGURE 10. CURVE-FIT TO THE TERM PROPORTIONAL TO $(KH)^4$ ON THE RHS OF EQ. (71)

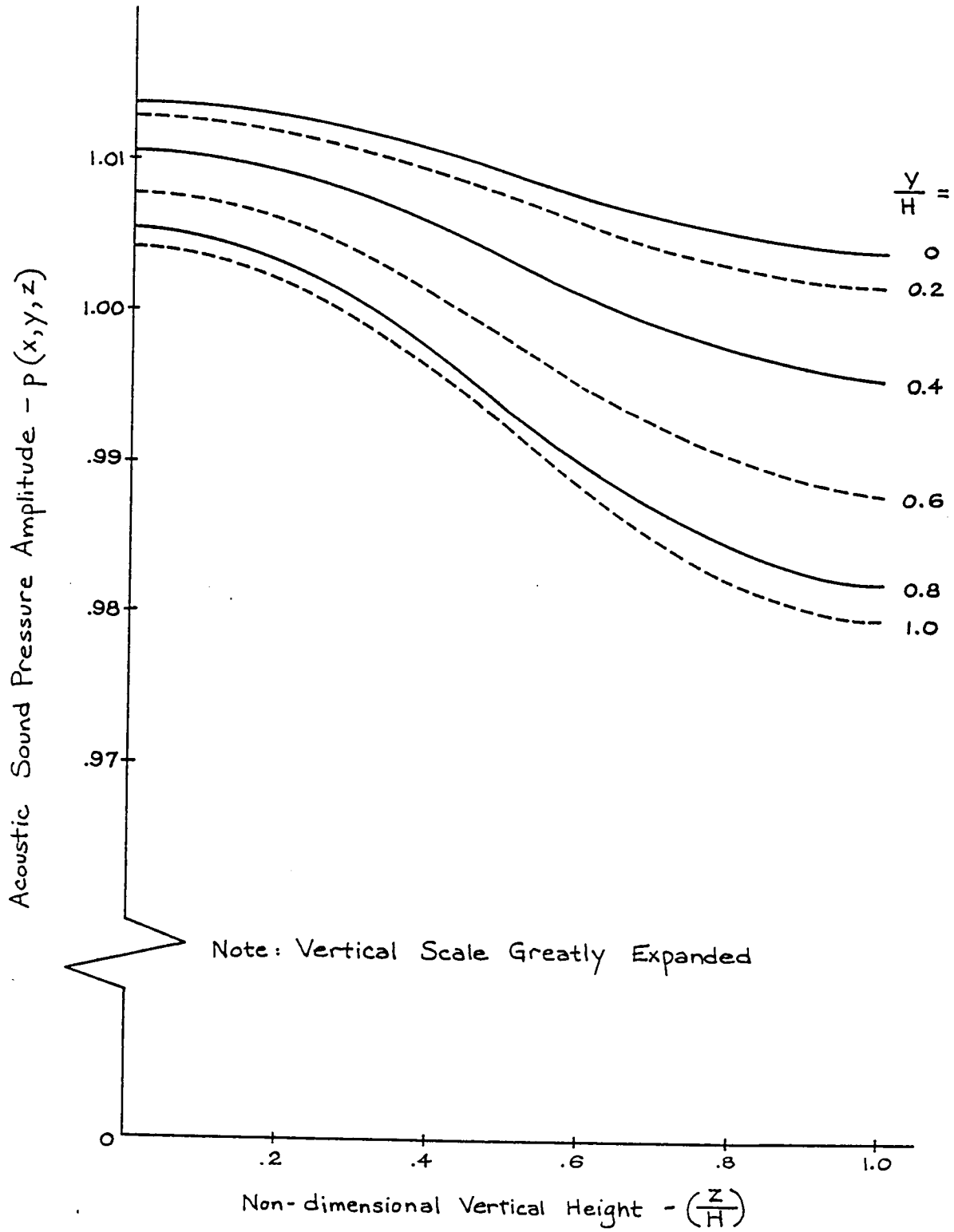

FIGURE 11. EFFECT OF REFRACTION ON THE ACOUSTIC PRESSURE DISTRIBUTION ACROSS DUCT FOR THE CASE KH=1 AND M_c=0.2

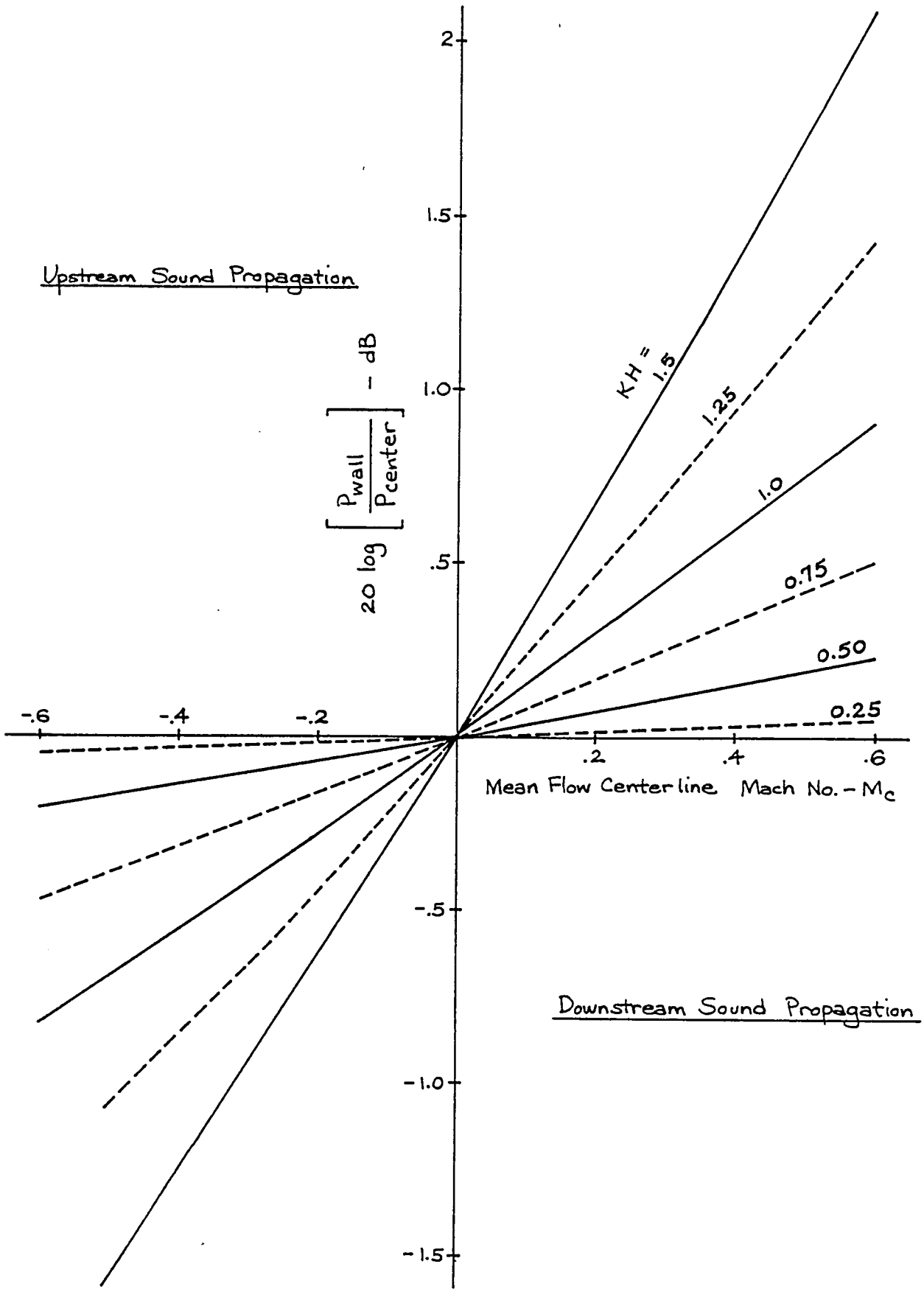

FIGURE 12. EFFECT OF FLOW AND SOUND FREQUENCY ON THE RATIO OF WALL TO CENTERLINE ACOUSTIC PRESSURE